NANO LETTERS

Letter

pubs.acs.org/NanoLett

A Robust and Facile Approach To Assembling Mobile and Highly-Open Unfrustrated Triangular Lattices from Ferromagnetic Nanorods

Maneesh K. Gupta, Dhaval D. Kulkarni, Ren Geryak, Swati Naik, and Vladimir V. Tsukruk*

School of Materials Science and Engineering, Georgia Institute of Technology, Atlanta, Georgia 30332, United States

Supporting Information

ABSTRACT: A simple and widely applicable approach to assemble long-range two-dimensional mobile arrays of functionalized nickel nanorods with tunable and "highly open" lattice structures is presented. The magnetic assembly of uniformly oriented nanorods in triangular lattices was achieved by a phase separation of the surface confined yet mobile vertical nanorods driven by a gradient magnetic field. In contrast to known approaches, the unfrustrated lattices can be further locked in place allowing for the removal of the applied magnetic field and processing without disrupting the initial order with different symmetries precisely assembled and locked in their position on the same substrate. We suggest that the tunable assemblies of magnetic nanorods provide a versatile platform for downstream handling of open lattice arrays for eventual device integration.

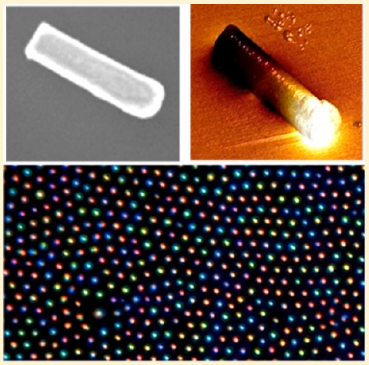

KEYWORDS: *Magnetic nanorods, field-assisted assembly, dynamic lattices, tunable assembly, open nanorod lattices*

The fabrication of organized polymer and colloidal arrays with easily tunable lattice spacing and symmetry is uniquely challenging due to self-assembly processes typically being driven and stabilized by mid- to short-range interactions such as electric double-layer repulsion, van der Waals attraction, and steric repulsion.[1] Thus, a vast majority of traditionally assembled colloidal systems have a simple close-packed structure with limited selection of lattice spacings and local symmetry defined by particle size, shape, and charge properties and intimate contact of the building blocks.[2−5]

On the other hand, materials strategies to achieve open, tunable, and complex-ordered lattices and structures with potentially unique physical properties include colloidal epitaxy,[6,7] binary colloidal mixtures,[8] template-assisted confinement,[9−12] Janus or patchy functionalization,[13−16] and the use of biomolecular/polymeric linkers or surfactants.[17−21] While interesting and useful, these approaches tend to be multistep, low-yield, and often require time-consuming design of materials systems including synthesizing complex linkers (e.g., complementary DNA strands),[17−20] processing multicomponent mixtures (e.g., nanoparticles and surfactants),[8] or achieving cumbersome selective functionalization of particles (e.g., site-specific grafting or modification).[13,15,16] For bottom-up assembly processes to truly rival conventional top-down fabrication in technological importance, novel strategies that leverage long-range forces and allow for easy fabrication of highly open structures with tunable and mobile lattices are crucial.

The application of external electric and magnetic fields can organize colloidal micro- and nanoparticles into ordered open lattices based on long-range interactions between induced or permanent electric or magnetic dipoles.[22−29] Numerous studies have demonstrated that the modulation of magnetic fields can lead to precise control over the lattice structure in one- and two-dimensional arrays.[30−32] However, a major limitation for such methods is that these particles preferentially form chains in the field direction with weak correlation between adjacent chains.[33,34] The lack of ordering arises from the varying dipole magnitudes among the inherently polydisperse chains in unconfined systems. This is typically overcome by utilizing physical confinement to prevent chaining altogether or only allowing the formation of monodisperse chain lengths. While the addition of physical confinement enables efficient formation of highly ordered arrays, this requirement presents its own challenges. For example, assemblies formed at the air−liquid or liquid−liquid interfaces dissipate the moment the external field is removed.[30,31] These restrictions limit the attractiveness of field-assisted assembly methods of micro-nanostructures, especially in scenarios where it is desired to assemble particles *in situ*.

In contrast to current methods, the approach suggested here enables the magnetic field-assisted assembly of chemically functionalized magnetic nanostructures, nickel nanorods, into long-range ordered and tunable 2D lattices directly at a substrate surface using a simple magnetic system and eliminating the need for any physical confinement beyond the substrate surface. Careful control of the nanorod concentration and deposition method allows for the formation of a metastable ferromagnetic monolayer of vertically oriented

Received: September 2, 2012
Revised: December 12, 2012
Published: December 13, 2012

   dx.doi.org/10.1021/nl303268s | *Nano Lett.* 2013, 13, 36−42

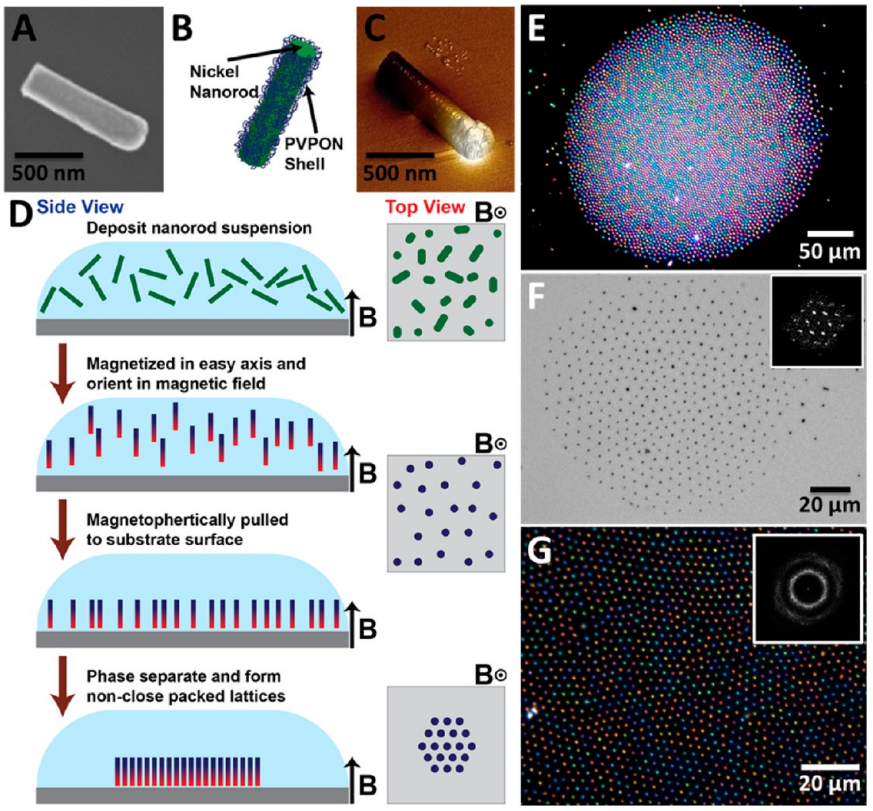

Figure 1. Assembly of nickel nanorods in an orthogonal magnetic field gradient. (A) SEM image of a 200 by 800 nm nanorod; (B) illustration of a PVPON coated nickel nanorod; (C) magnetic force microscopy image showing the persistent magnetic dipole on a nanorod after removal from an external magnetic field; (D) Schematic showing a cross-sectional and top-down perspective of the proposed nanorod assembly process; (E,F) optical microscopy images showing (E) a well-formed island imaged under dark field and (F) a smaller assembly imaged under bright field with corresponding FFT; (G) an assembly imaged at high-magnification under dark field with corresponding FFT.

nanorods. In the assembled state, the nanorods form an extremely open and unfrustrated triangular lattice with the spacing between nanorods exceeding their diameter by nearly 2 orders of magnitude.

We demonstrate control over the lattice spacing and symmetry by varying the magnitude and orientation of the magnetic field. The direct assembly of the nanorods at the solid−liquid interface further facilitates anchoring of the nanorods to the substrate through triggered intermolecular interactions enabling preservation of the assembled array even after removing the magnetic field. Immobilizing the nanorods in this way opens possibilities including hierarchical and sequential assembly of multiple lattices in close proximity to each other, and rapid actuation of the nanorod arrays similar to artificial cilia in external flow[35] by changing the magnetic field orientation.

The functionalized nickel nanorods used for field-assisted assembly were made by the well-known template-assisted technique based on infiltration or electrodeposition in porous anodic alumina templates (see Supporting Information).[36−39] The advantage of this technique is that it allows for high throughput and uniform fabrication of nanotubes and nanorods from inorganic and organic materials with adjustable dimensions.[40] The lengths of the rods were varied by adjusting the duration of electrodeposition, resulting in rods with lengths between 400 and 1600 nm (Figure 1A shows an 800 nm long nanorod). Individual nanorods were obtained by dissolving away the alumina membrane and coated with a layer of polyvinylpyrrolidone (PVPON) to prevent fast aggregation in solution (Figure 1B).

Nickel nanorods in this dimension range and made with similar techniques have been shown to be ferromagnetic with a saturated magnetization close to the bulk value of nickel (485 emu/cm^3).[41] Since all of the rods used in the study have an aspect ratio much greater than one (ranging from 2 to 8), they have an easy axis of magnetization along the long axis of the rod. Indeed, magnetic force microscopy (MFM) of a magnetized nanorod obtained in a lift mode with magnetic tip[42] shows a contrast in the phase shift along the length of the rod thus confirming that the strong magnetic dipole moment is aligned with the nanorod's long-axis as reflected by changing color (Figure 1C).

Upon placement of the nanorod suspension in a vertical magnetic field the nanorods are quickly magnetized and orient perpendicular to the substrate surface (Figure 1D). The placement of the magnet creates a steep gradient in magnetic flux density normal to the substrate that results in a magnetophoretic force pulling the nanorods: from the suspension to the surface (Supporting Information Figure S1).[43,44] Once on the surface, the nanorods maintain high lateral mobility and undergo a "phase separation" that results in the formation of stable labyrinth or island-like morphology. On larger diameter magnets (diameter >1 cm), the nanorods were found to first form a labyrinth morphology that coarsened over time to eventually form discrete islands (Supporting Information Figure S2). However, by using smaller magnets (diameter <1 cm) the assembly could be controlled so that only

dx.doi.org/10.1021/nl303268s | Nano Lett. 2013, 13, 36−42

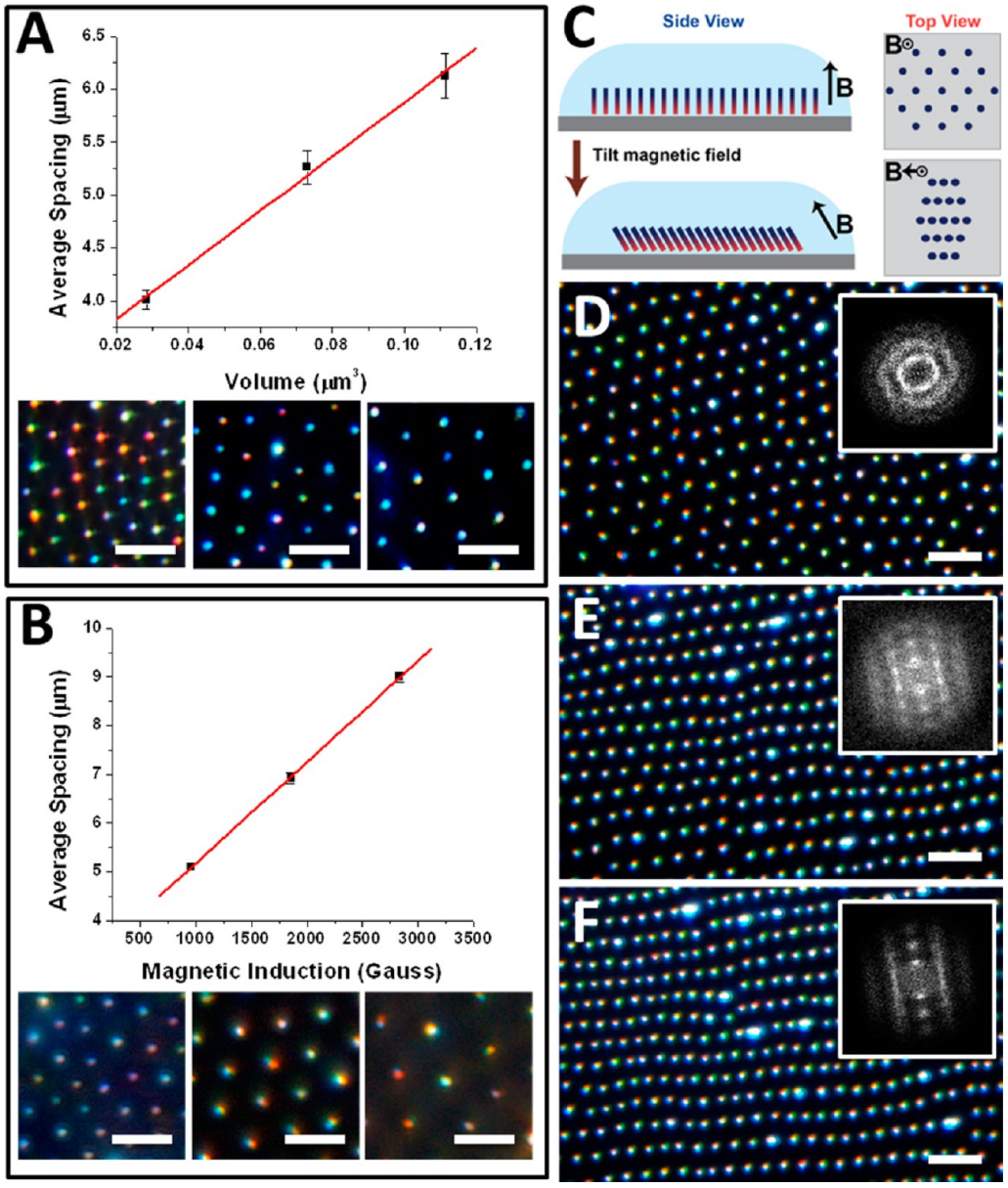

Figure 2. Tunability of lattice spacing and symmetry. (A) The linear relationship between nickel nanorod volume and the equilibrium rod spacing in the assemblies. Inset images are shown (left to right) for 0.0126, 0.0251, and 0.0503 μm^3. (B) The linear relationship between applied magnetic field and the equilibrium rod spacing in the assemblies. Inset images are shown (left to right) for 900, 1800, and 2700 G applied field. (C) A cross-sectional and top-down perspective of the effect of an orthogonal and nonorthogonal field on the rod assemblies. (D−F) Sequential dark-field optical microscopy images of rods as magnetic field is tilted and corresponding FFTs: (D) orthogonal field, (E,F) tilted fields.

a single island was formed in response to the radial gradients in magnetic flux density. Using this method, the nanorods are preferentially concentrated at the center of the magnet, and the position of the island can be precisely controlled by placement of the magnet center.

In this process, individual nanorods continually "arrive" from the bulk solution phase and slowly incorporate themselves at the island boundaries until depleted as can be observed in real-time (Figure 1E, Supporting Information Video S1). Interestingly, within the aggregated phase the nanorods are packed into an extremely open and ordered hexagonal lattice with long-range positional order indicated by 6-fold symmetry in the FFT with up to third order of Fourier components visible (Figure 1F,G). We observed that a dilute suspension of nanorods can be used to avoid the formation of chain aggregates within the island. At higher concentrations (>10^6 nanorods/mL), the chain aggregates in the island dramatically impact the quality of the lattice ordering as these aggregates have a larger dipole moment observed by a larger clearing zone. Therefore, reducing the concentration to below 2.5 × 10^5 nanorods/mL resulted in the formation of monolayer islands with excellent lateral long-range ordering (Supporting Information Figure S3). Moreover, the individual island size can be tightly controlled over a wide range by varying the total amount of nanorods from small islands, containing fewer than 20−50 nanorods, all the way up to large-scale islands with 500 μm diameter, containing more than 25 000 nanorods (Supporting Information Figure S4). The placement of the island could be manipulated precisely after formation as the entire island could be moved efficiently and continuously by slowly moving the

dx.doi.org/10.1021/nl303268s | *Nano Lett.* 2013, 13, 36−42

magnet in relation to the substrate (Supporting Information Video S2). Real-time lateral movement of the nanorods with reconfiguration of local organization, deformational flow around defects, and continuous reformation of the island front are clearly visible in the video.

The field-assisted formation of lattices with spacing incommensurately larger than size of the individual elements is facilitated by the long-range repulsive forces arising from the uniformly aligned magnetic dipole moments of the nanorods (ferromagnetic ordering).[30] As known, frustrated triangular lattices can be formed by magnetic dipoles that are free to change their dipole orientation through flipping.[45] Such flipping events minimize the overall magnetic energy of unconfined lattices and facilitate formation of triangular symmetry with lattice spacing (d) comparable to the magnetic dipole length (l): $d \sim l$. In striking contrast, the kinetically confined spatial conditions at the solid−liquid interface and the externally applied field cause the nanorods to lose the freedom to flip. Thus, the only physical pathway to magnetic energy minimization is lateral displacement to form unfrustrated and highly open lattices with a unique $d \gg l$ characteristic, which is rarely observed in synthetic colloidal systems. Dramatically increasing spacing minimizes repulsive interactions and continues until it is balanced by the much weaker chemical potential, stabilizing at distances about 2 orders of magnitude larger than the diameter of the nanorods.

The repulsive long-range forces provide a means for wide range tunability of the lattice spacing and symmetry. Increasing the magnetic moment of the nanorods through an increase in either the volume or the magnetization of the nanorods will lead to an increase in the magnetostatic repulsive force and consequently larger lattice spacing. As known, the magnetic field H_x created by a dipole with moment m and length l, at a distance x in the direction perpendicular to the dipole, is given by

$$H_x = \frac{m}{\left(x^2 + \frac{l^2}{4}\right)^{3/2}} \quad (1)$$

where the magnetic moment is $m = MV$, and M and V are, respectively, the magnetization and volume of the nanorod.[41] This dipole approximation gives a valuable estimation of the magnitude of the magnetostatic forces between nanorods with different characteristics. To test this relationship, nanorods with lengths of 400, 800, and 1600 nm (constant diameter of 200 nm) were fabricated and assembled on a cylindrical magnet with surface field strength of 900 G. Figure 2A shows optical images of the resulting lattices and a plot of lattice spacing versus rod volume. As expected from eq 1, it is found that the spacing increases linearly over the range of 4 to 6.5 μm with the increase in nanorod volume. On the basis of the saturated magnetization of nickel (485 emu/cm^3), we find that field strength for each nanorod length at the respective equilibrium lattice spacing was fairly constant and between 8 and 9 Oersted (Supporting Information Figure S5). This indicates that the repulsive force at the equilibrium lattice spacing is virtually constant over this range of rod lengths.

Similarly, increasing the magnetization of the nanorods should increase the perpendicular field and also the repulsive force in accordance with eq 1. To test this relationship, 800 nm long rods were assembled on magnets with surface-field strengths of 900, 1800, and 2800 G and the resulting lattice spacing was measured (Figure 2B). It was found that the lattice spacing increased linearly with the increase in magnetic field indicating that the field strengths of the magnets are above the saturation field of nickel at which point the susceptibility becomes nearly constant. Thus, an increase in the external field leads to corresponding increase in the magnetic moment of the nanorods.

Next, tilting the external magnetic field with respect to the substrate plane easily reorients the nanorods to maintain the axis of magnetization in the field direction. As a result, the repulsive force between adjacent rods becomes anisotropic and the nanorods form a rhombic lattice with the reduced lattice parameter in the direction of the tilted magnetic field (Figure 2C). In Figure 2D−F, the optical images show the effect of sequential tilting of the external magnetic field on the lattice geometry in an assembled island, and as expected the lattice geometry shifts from triangular (Figure 2D) to rhombic (Figure 2E) as confirmed by FFT images. This is due to the weakening of the repulsive forces with the decrease in the distance between the opposite magnetic poles in adjacent nanorods. Further increase in the magnetic field angle with respect to the substrate normal results in a decrease in the lattice spacing with the preservation of strong interchain correlations of magnetic nanorods (Figure 2F) in contrast to uncorrelated chains of spherical nanoparticles magnetically assembled.[46]

As mentioned earlier, one of the major challenges facing field-assisted assembly methods is the difficulty in maintaining the assembled arrays in integrated materials/structures when the assisted field is turned off. In fact, as expected, without further processing to anchor or encapsulate the nanorods removal of the magnetic field leads to irreversible chain formation (Figure 3A) due to the strong remnant magnetization of the ferromagnetic nanorods and preferred pole-to-pole interactions. Once this happens, the array cannot be recovered even when the magnetic field is reapplied. Since the nanorod array is assembled and anchored directly at the substrate surface, the close proximity of the nanorods with the substrate enables strategies for robust encapsulation and preservation of the nanorod arrays. A second major advantage is that the assembled arrays can be further incorporated in

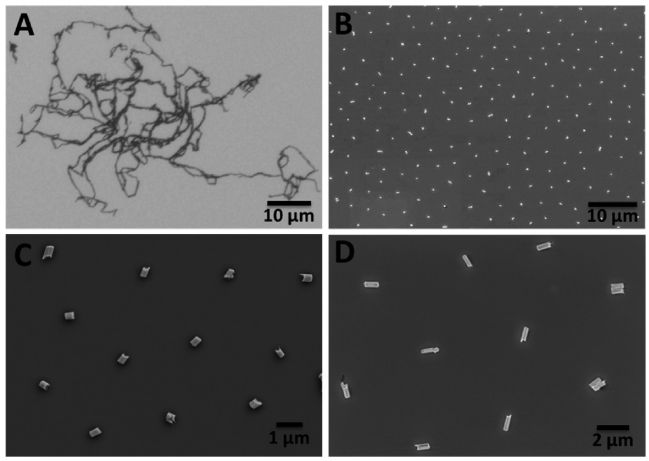

Figure 3. Tethering of nanorod arrays to the substrate. (A) Bright-field optical image demonstrating the effect of removing the external field without tethering nanorods. (B−D) SEM images showing tethered nanorods after external fields have been removed, (B) large area view of 400 nm length rods, (C) close-up image of 400 nm length rods, and (D) close up image of 800 nm length rods.

dx.doi.org/10.1021/nl303268s | Nano Lett. 2013, 13, 36−42

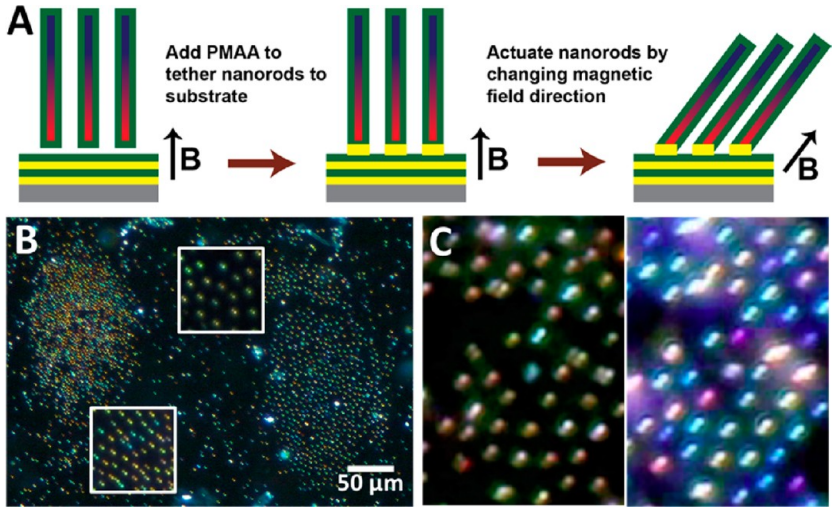

Figure 4. Sequential deposition of hierarchical assemblies and actuation of arrays. (A) Schematic showing tethering process based on hydrogen-bonding between PMAA and PVPON layers. (B) Dark-field optical image showing sequential deposition of two islands on the same substrate left island is comprised of 400 nm long nanorods and right-side island of 800 nm long rods. (C) Dark-field images from movie S3 showing the change in scattering intensity as nanorods are actuated by an external magnetic field.

flexible media using conventional processes such as monomer polymerization as introduced briefly in Supporting Information and will be further discussed elsewhere. Such processing is challenging for conventional systems utilizing electromagnetic coils and fluid cells due to the bulky nature of the coils and the need to maintain precise placement of the array within the coil/cell.

In an attempt to preserve the field-induced organization, we modified the chemical composition of the dispersion and changed the balance of nanorod-surface interactions. We suggested that adding dilute salt solutions (25 mM NaCl) to the nanorod array might decrease charge screening between the nanorods and the silicon substrate allowing the PVPON shells on the nanorods to physically adsorb to the substrate (Supporting Information Videos S1, S2). While this simple addition could freeze the nanorods, the anchoring was very weak as even mild rinsing dramatically disturbed the ordered arrays. Therefore, we developed a hydrogen-bonding based anchoring approach by introducing polymethacrylic acid/PVPON (PMAA/PVPON) functionalized substrates.[47,48] In this design, dilute solutions of PMAA were added dropwise to arrays formed in order to facilitate hydrogen-bond anchoring of PVPON-functionalized nanorod ends and substrate and the firm preservation of the initial ordering even after drying and rinsing processes (Figures 3B–D, 4A).

Moreover, the robust nature of the hydrogen-bonded coupling allowed deposition of multiple islands with different lattices on the same substrate by repeating the assembly process at different locations (Figure 4B). Here, the island on the left side of the image is comprised of 400 nm long nanorods, and the island on the right side contains 800 nm long nanorods. As shown in Figure 2A, the island containing longer nanorods has larger lattice spacing. The precise placement of the second island was achieved by registry of the desired location with the magnet center. The ability to sequentially deposit multiple islands with precise control of the island spacing could allow such a technique to be adopted for fabrication of multiplexed arrays for application in biological and chemical sensing. Furthermore, this method can easily be extended to a wide variety of shells with hydrogen-bonding, electrostatic interactions, or even covalent cross-linking.

An interesting consequence of the coupling method utilized here is that the polymer chains placed in-between the nanorod ends and the substrate can act as hinges about which the nanorods can freely rotate (Figure 4A). In this way, changing the magnetic field orientation leads to rapid actuation of the nanorod array in a manner similar to artificial cilia on flexible supports[49] and in contrast to microfabricated rod arrays that can only actuate via bending modes.[50−52] In Figure 4c and Supporting Information Video S3 the fast, real-time actuation of the nanorod array can be seen by the dramatic shift in the color and intensity of the scattered light. Changing the orientation of the nanorods from vertically standing to tilted increases the scattering cross-section, and this is readily observed in the dark-field optical video.

The results presented here demonstrate a unique assembly of nickel nanorods into long-range organized lattices with tunable spacing and symmetry using a gradient magnetic field. Once at the substrate interface, the nanorods undergo a phase separation forming highly open unfrustrated lattices, whose structure is governed by the long-range repulsive forces between the uniformly oriented adjacent magnetic dipoles. We suggest that the high interfacial mobility of the nanorods along with long-range repulsion of kinetically confined magnetic dipoles resulted in the formation of unfrustrated triangular lattices with spacing between vertical nanorods exceeding their diameter by a ratio of 50:1 and open volume exceeding 99.9%. This assembly process is facilitated by the combination of magnetophoretic assembly, high lateral mobility of nanorods, kinetic confinement, and field/concentration-controlled phase separation. In contrast to ferrofluids and magnetorheologic fluids in a thin cell, which undergo phase separation when placed in orthogonal magnetic fields,[53,54] a fluid cell confinement is not required in current approach.

These open lattices can be further locked in position by the triggering of hydrogen-bonding between the funcationalized nanorods and the substrate. This anchoring technique was extended to allow for assembly of multiple lattices with different geometries and spacing on the same substrate with

dx.doi.org/10.1021/nl303268s | *Nano Lett.* 2013, 13, 36−42

precise registry. Furthermore, the hingelike polymeric anchors offer the possibility to rapidly actuate the nanorods in a manner similar to artificial cilia.[35,49] Thus, the magnetic-field assisted assembly of nanorods demonstrated here offers a unique combination of ease of assembly and ease of integration making it a promising platform for self-assembly in a wide range of applications including rapidly actuating arrays for micromixing/manipulation, biological/chemical sensing, and active magneto/optical/photonic systems. Compared to other self-assembled or lithographically fabricated post arrays this approach offers the advantage that long-range ordered arrays with uniform cilia lengths can be easily assembled *in situ* without the need for complex physical confinement. Moreover, the ease of integrating other materials offers the possibility of creating magnetically actuated ferromagnetic arrays with fast-responsive multifunctional actuating behavior.

■ ASSOCIATED CONTENT

Supporting Information

Methods, Figures S1−S5, and three video files. This material is available free of charge via the Internet at http://pubs.acs.org.

■ AUTHOR INFORMATION

Corresponding Author

*E-mail: vladimir@mse.gatech.edu.

Notes

The authors declare no competing financial interest.

■ ACKNOWLEDGMENTS

This work is funded through the BIONIC center sponsored by the Air Force Office of Scientific Research and the Air Force Research Laboratories under contract numbers FA9550-11-1-0233 and FA9550-09-1-0162. We would like to thank Dr. R. Vaia for helpful discussions and feedback and Dr. K. Kornev for characterization of rare earth magnets.

■ REFERENCES

(1) Bishop., J. M. K.; Wilmer, C. E.; Soh, S.; Grzybowski, B. A. *Small* **2009**, *5*, 1600−1630.
(2) Anderson, V. J.; Lekkerkerker, H. N. W. *Nature* **2002**, *416*, 811−815.
(3) Glotzer, S. C.; Solomon, M. J. *Nat. Mater.* **2007**, *6*, 557−562.
(4) Ye, X.; Qi, L. *Nano Today* **2011**, *6*, 608−631.
(5) Tsukruk, V. V. *Prog. Polym. Sci.* **1997**, *22*, 247−277.
(6) van Blaaderen, A.; Ruel, R.; Wiltzius, P. *Nature* **1997**, *385*, 321−324.
(7) Hoogenboom, J. P.; van Langen-Suurling, A. K.; Romijn, J.; van Blaaderen, A. *Phys. Rev. Lett.* **2003**, *90*, 138301.
(8) Shevchenko, E. V.; Talapin, D. V.; Kotov, N. A.; O'Brien, S.; Murray, C. B. *Nature* **2006**, *439*, 55−59.
(9) Yin, Y.; Lu, Y.; Gates, B.; Xia, Y. *J. Am. Chem. Soc.* **2001**, *123*, 8718−8729.
(10) Xia, Y.; Yin, Y.; Lu, Y.; McLellan, J. *Adv. Funct. Mat.* **2003**, *13*, 907−918.
(11) Singamaneni, S.; McConney, M. E.; Tsukruk, V. V. *Adv. Mater.* **2010**, *22*, 1263−1268.
(12) Singamaneni, S.; McConney, M. E.; Tsukruk, V. V. *ACS Nano* **2010**, *4*, 2327−2337.
(13) Chen, Q.; Bae, S. C.; Granick, S. *Nature* **2011**, *469*, 381−385.
(14) Smoukov, S. K.; Gangwal, S.; Marquez, M.; Velev, O. D. *Soft Matter* **2009**, *5*, 1285−1292.
(15) Nie, Z.; Fava, D.; Rubinstein, M.; Kumacheva, E. *J. Am. Chem. Soc.* **2008**, *130*, 3683−3689.
(16) Anderson, K. D.; Luo, M.; Jakubiak, R.; Naik, R. R.; Bunning, T. J.; Tsukruk, V. V. *Chem. Mater.* **2010**, *22*, 3259−3264.
(17) Alivisatos, A. P.; Johnsson, K. P.; Peng, X.; Wilson, T. E.; Loweth, C. J.; Bruchez, M. P., Jr.; Schultz, P. G. *Nature* **1996**, *382*, 609−611.
(18) Park, S. Y.; Lytton-Jean, A. K. R.; Lee, B.; Weigand, S.; Schatz, G. C.; Mirkin, C. A. *Nature* **2008**, *451*, 553−556.
(19) Nykpanchuk, D.; Maye, M. M.; van der Lelie, D.; Gang, O. *Nature* **2008**, *451*, 549−552.
(20) Macfarlane, R. J.; Lee, B.; Jones, M. R.; Harris, N.; Schatz, G. C.; Mirkin, C. A. *Science* **2011**, *334*, 204−208.
(21) Guerrero-Martinez, A.; Perez-Juste, J.; Carbo-Argibay, E.; Tardajos, G.; Liz-Marzan, L. M. *Angew. Chem., Int. Ed.* **2009**, *48*, 9484−9488.
(22) Rogach, A. L.; Kotov, N. A.; Koktysh; Ostrander, J. W.; Ragoisha, G. A. *Chem. Mater.* **2000**, *12*, 2721−2726.
(23) Giersig, M.; Mulvaney, P. *Langmuir* **1993**, *9*, 3408−3413.
(24) Trau, M.; Saville, D. A.; Aksay, I. A. *Science* **1996**, *272*, 706−709.
(25) Lumsdon, S. O.; Kaler, E. W.; Williams, J. P.; Velev, O. D. *Appl. Phys. Lett.* **2003**, *82*, 949−951.
(26) Golosovsky, M.; Saado, Y.; Davidov, D. *Phys. Rev. E* **2002**, *65*, 061405.
(27) Alsberg, E.; Feinstein, E.; Joy, M. P.; Prentiss, M.; Ingber, D. E. *Tissue Eng.* **2006**, *12*, 3247−3256.
(28) Pregibon, D. C.; Toner, M.; Doyle, P. S. *Langmuir* **2006**, *22*, 5122−5128.
(29) Hangarter, C. M.; Rheem, Y.; Yoo, B.; Yang, E.-H.; Myung, N. V. *Nanotechnology* **2007**, *18*, 205305.
(30) Wen, W.; Zhang, L.; Sheng, P. *Phys. Rev. Lett.* **2000**, *85*, 5464−7.
(31) Grzybowski, B. A.; Stone, H. A.; Whitesides, G. M. *Nature* **2000**, *405*, 1033−1036.
(32) Motornov, M.; Malynych, S. Z.; Pippalla, D. S.; Zdyrko, B.; Royter, H.; Roiter, Y.; Kahabka, M.; Tokarev, A.; Tokarev, I.; Zhulina, E.; Kornev, K. G.; Luzinov, I.; Minko, S. *Nano Lett.* **2012**, *12*, 3814−3820.
(33) Keng, P. Y.; Shim, I.; Korth, B. D.; Douglas, J. F.; Pyun, J. *ACS Nano* **2007**, *1*, 279−292.
(34) Bowles, S. E.; Wu, W.; Kowalewski, T.; Schalnat, M. C.; Davis, R. J.; Pemberton, J. E.; Shim, I.; Korth, B. D.; Pyun, J. *J. Am. Chem. Soc.* **2007**, *129*, 8694−8695.
(35) McConney, M. E.; Chen, N.; Lu, D.; Hu, H. A.; Coombs, S.; Liu, C.; Tsukruk, V. V. *Soft Matter* **2009**, *5*, 292−295.
(36) Martin, C. R. *Science* **1994**, *266*, 1961−1966.
(37) Hulteen, J. C.; Martin, C. R. *J. Mater. Chem.* **1997**, *7*, 1075−1087.
(38) Banholzer, M. J.; Qin, L.; Millstone, J. E.; Osberg, K. D.; Mirkin, C. A. *Nat. Protoc.* **2009**, *4*, 838−848.
(39) Chang, S.; Singamaneni, S.; Kharlampieva, E.; Young, S. L.; Tsukruk, V. V. *Macromolecules* **2009**, *42*, 5781−5785.
(40) Jones, M. R.; Osberg, K. D.; Macfarlane, R. J.; Langille, M. R.; Mirkin, C. A. *Chem. Rev.* **2011**, *111*, 3736−3827.
(41) Sun, L.; Hao, Y.; Chien, C.-L.; Searson, P. C. *IBM J. Res. Dev.* **2005**, *49*, 79−102.
(42) McConney, M. E.; Singamaneni, S.; Tsukruk, V. V. *Polym. Rev.* **2010**, *50*, 235−286.
(43) Lim, J.; Tan, D. X.; Lanni, F.; Tilton, R. D.; Majetich, S. A. *J. Magn. Magn. Mater.* **2009**, *321*, 1557−1562.
(44) Lim, J.; Lanni, C.; Evarts, E. R.; Lanni, F.; Tilton, R. D.; Majetich, S. A. *ACS Nano* **2011**, *5*, 217−226.
(45) Wang, R. F.; Nisoli, C.; Freitas, R. S.; Li, J.; McConville, W.; Cooley, B. J.; Lund, M. S.; Samarth, N.; Leighton, C.; Crespi, V. H.; Schiffer, P. *Nature* **2006**, *439*, 303−306.
(46) Singamaneni, S.; Bliznyuk, V. N.; Binek, C.; Tsymbal, E. Y. *J. Mater. Chem.* **2011**, *21*, 16819−16845.
(47) Kharlampieva, E.; Kozlovskaya, V.; Sukhishvili, S. A. *Adv. Mater.* **2009**, *21*, 3053−3065.
(48) Kozlovskaya, V.; Kharlampieva, E.; Khanal, B. P.; Manna, P.; Zubarev, E. R.; Tsukruk, V. V. *Chem. Mater.* **2008**, *20*, 7474−7485.
(49) McConney, M. E.; Anderson, K. D.; Brott, L. L.; Naik, R. R.; Tsukruk, V. V. *Adv. Funct. Mater.* **2009**, *19*, 2527−2544.

(50) Singh, H.; Laibinis, P. E.; Hatton, T. A. *Nano Lett.* **2005**, *5*, 2149−2154.
(51) Evans, B. A.; Shields, A. R.; Carroll, R. L.; Washburn, S.; Falvo, M. R.; Superfine, R. *Nano Lett.* **2007**, *7*, 1428−1434.
(52) Sidorenko, A.; Krupenkin, T.; Taylor, A.; Fratzl, P.; Aizenberg, J. *Science* **2007**, *315*, 487−490.
(53) Andelman, D.; Rosensweig, R. E. *J. Phys. Chem. B* **2009**, *113*, 3785−3798.
(54) Wolf, H.; Birringer, R. *J. Appl. Phys.* **2005**, *98*, 074303.

dx.doi.org/10.1021/nl303268s | *Nano Lett.* 2013, 13, 36−42